

Multiphase flow characteristics of heterogeneous rocks from CO₂ storage reservoirs in the United Kingdom

Catriona A. Reynolds¹, Martin J. Blunt¹, Samuel Krevor¹

¹Department of Earth Science and Engineering, Imperial College London, London, United Kingdom

Key Points:

- CO₂-brine flow and trapping was evaluated for three rocks from target CO₂ storage reservoirs in the UK
- The impact of heterogeneity was observed by varying N_c while visualising the fluid distribution and measuring relative permeability
- Small scale rock heterogeneity has a major impact on multiphase flow properties for CO₂ storage, and should be measured quantitatively

Corresponding author: Samuel Krevor, s.krevor@imperial.ac.uk

Abstract

We have studied the impact of heterogeneity on relative permeability and residual trapping for rock samples from the Bunter sandstone of the UK Southern North Sea, the Ormskirk Sandstone of the East Irish Sea, and the Captain Sandstone of the UK Northern North Sea. Reservoir condition CO₂-brine relative permeability measurements were made while systematically varying the ratio of viscous to capillary flow potential, across a range of flow rates, fractional flow, and during drainage and imbibition displacement. This variation resulted in observations obtained across a range of core-scale capillary number $0.2 < N_c = \frac{\Delta P}{L} \frac{H}{\Delta P_c} < 200$. Capillary pressure heterogeneity was quantitatively inferred from 3D observations of the fluid saturation distribution in the rocks. For each of the rock samples a threshold capillary number, $5 < N_c < 30$, was found, below which centimetre-scale layering resulted in a heterogeneous distribution of the fluid phases and a commensurate impact on flow and trapping. The threshold was found to be dependent on the capillary number alone, irrespective of the displacement path (drainage or imbibition) and average fluid saturation in the rock. The impact of the heterogeneity on the relative permeability varied depending on the characteristics of the heterogeneity in the rock sample, whereas heterogeneity increased residual trapping in all samples above what would be expected from the pore-scale capillary trapping mechanism alone. Models of subsurface CO₂ injection should use properties that incorporate the impacts of heterogeneity at the flow regime of interest or risk significant errors in estimates of fluid flow and trapping.

1 Introduction

Predictions of the flow behaviour and storage capacity of CO₂ in subsurface reservoirs are sensitive to the underlying multiphase flow properties of the system [Mathias *et al.*, 2013; Yoshida *et al.*, 2016; Szulczewski *et al.*, 2012]. These are primarily the capillary pressure, relative permeability, and residual trapping characteristics. Site-specific coreflood measurements are a requirement for accurate estimates of the plume migration and storage capacity obtained through reservoir simulation.

A large number of measurements of reservoir condition CO₂-brine relative permeability and trapping have been reported in the literature [Burnside and Naylor, 2014; Benson *et al.*, 2013]. Many of the studies primarily used quarry rocks to establish general properties of the CO₂-brine multiphase flow system. These have shown that CO₂ acts as a non-wetting fluid similar to other non-aqueous fluids, and that there is significant capillary trapping [Krevor *et al.*, 2012; Akbarabadi and Piri, 2013; Manceau *et al.*, 2015; Reynolds and Krevor, 2015]. Site-specific data, in contrast, is primarily limited to locations in the United States and Canada [Krevor *et al.*, 2012; Bennion and Bachu, 2008]. As a result, many modelling studies make use of generic relative permeability curves, or curves selected from the literature dataset for a similar rock type.

In the UK there have been many suggestions for potential storage sites [Scottish Carbon Capture and Storage, 2012; Holloway *et al.*, 2006; Kirk, 2006; Brownsort *et al.*, 2015; Holloway and Savage, 1993; Scottish Carbon Capture and Storage, 2009; Haszeldine *et al.*, 2013; Brownsort *et al.*, 2015; Scottish Carbon Capture and Storage, 2009; Akhurst *et al.*, 2011]. However, prior to this work, only one CO₂-brine relative permeability curve was publicly available, from a measurement on a Bunter sandstone sample from the Southern North Sea, evaluated as a part of the 2008 CASSEM (CO₂ Aquifer Storage Site Evaluation and Monitoring) project [Smith *et al.*, 2012]. A primary goal of this work was to provide data for modelling studies of CO₂ storage in UK reservoir systems. We have measured drainage and imbibition relative permeability, and residual trapping in rock samples obtained for three important potential CO₂ storage locations.

A number of studies have also shown that small-scale rock heterogeneities have a significant impact on CO₂ flow, which propagates to larger scales. In laboratory core floods of CO₂ and brine, the fluids are commonly observed to distribute heterogeneously in the rock

Formation	Storage location	Well location	Well	Sample Depth [m]
Bunter	S. North Sea	onshore geothermal borehole	Cleethorpes-1	1312.7-1316.1
Ormskirk	E. Irish Sea	depleted gas field	Block 110/2a	1247.9-1248.1
Captain	N. North Sea	offshore hydrocarbon borehole	14/29a-3	2997.6-3005.1

Table 1. Sample locations for the rock cores

cores during two-phase flow [Reynolds and Krevor, 2015; Hingerl et al., 2016]. The dominant control on steady-state fluid distribution at this scale is variation in capillary pressure [Zhou et al., 1997; Kuo and Benson, 2015]. It has been theorised that the impact of this heterogeneity on macroscopic flow will depend on the ratio of the viscous or buoyant force to gradients in the capillary pressure, expressed quantitatively using a continuum scale capillary number [Zhou et al., 1997; Pickup and Stephen, 2000; Virnovsky et al., 2004; Debbabi et al., 2017]. This framework has been used extensively in numerical upscaling studies to describe flow regimes in which heterogeneity may be significant. Observations in this study were designed to evaluate the varying impact of rock heterogeneity experimentally, through a systematic variation of the capillary number, throughout both drainage and imbibition displacement processes.

A number of studies have shown that capillary heterogeneity can be characterised in cylindrical rock samples with a combination of observations and numerical simulations [Kuo and Benson, 2015; Pini and Benson, 2013a; Krause et al., 2013; Egermann and Lenormand, 2005; Huang et al., 1995]. The effects of small scale capillary heterogeneity is manifested at larger scales through both fluid flow and trapping [Meckel et al., 2015; Gershenson et al., 2017; Saadatpoor et al., 2009; Debbabi et al., 2017]. If the underlying heterogeneity is characterised, these effects may be accounted for through the use of upscaled relative permeability and residual trapping models [Li and Benson, 2015; Rabinovich et al., 2015]. The laboratory characterisation, however, must be performed as a variation from the conventional special core analysis workflow (see McPhee et al. [2015] for a comprehensive overview of current practice in core analysis).

In characterising the multiphase flow properties of the samples from UK sites, we have endeavoured to replicate reservoir conditions of pressure, temperature, and brine salinity. Additionally, we used an extension of the conventional core analysis protocol, characterising CO₂-brine flow behaviour across a range of fluid flow velocities, fractional fluid flow, and during drainage and imbibition displacement. This allowed for a characterisation of capillary heterogeneity within the framework of the capillary-viscous flow regimes and a direct link to the impacts on the macroscopic fluid mobility (relative permeability) and trapping.

2 Rock samples

2.1 Sample locations

Three samples were selected from reservoir formations identified as potential CO₂ storage sites in the UK (Figure 1 and Table 1). In the wake of the 2005 IPCC Special Report on Carbon Dioxide Capture and Storage [Metz et al., 2005] which identified CCS as a major technology for mitigating climate change, criteria were established to aid the selection of suitable CO₂ storage sites around the UK [Chadwick et al., 2008]. In the Southern North Sea and East Irish Sea extensive Permo-Triassic sandstones were identified for saline aquifer storage [Scottish Carbon Capture and Storage, 2012; Holloway et al., 2006; Kirk, 2006; Brown-sort et al., 2015; Holloway and Savage, 1993; Scottish Carbon Capture and Storage, 2009; Haszeldine et al., 2013]. This included the Bunter Sandstone Formation (Triassic Sherwood

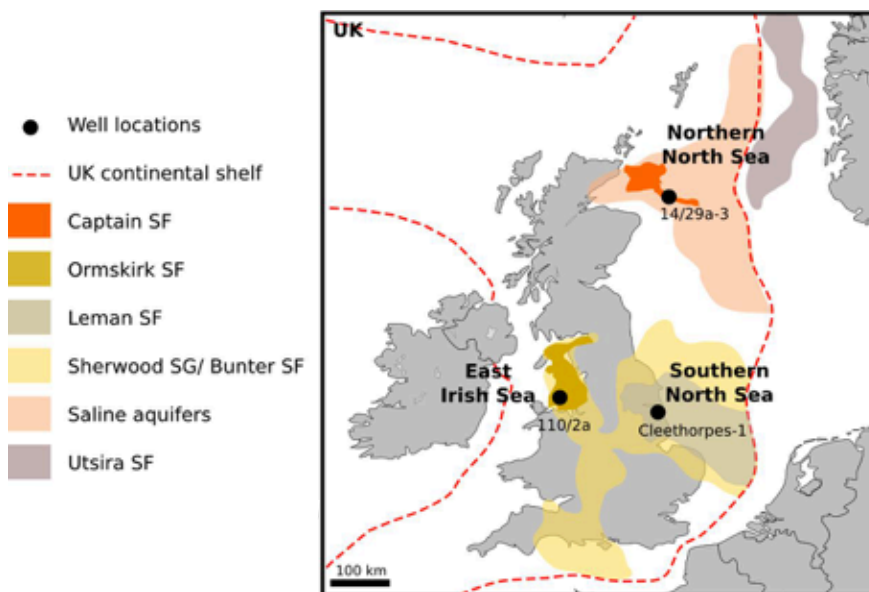


Figure 1. The well locations where samples were obtained.

Sandstone Group, Southern North Sea), Leman Sandstone Formation (Permian Rotliegend Sandstone Group, Southern North Sea) and Ormskirk Sandstone Formation (Triassic Sherwood Sandstone Group, East Irish Sea). In the Northern North Sea the Captain Sandstone Formation [Brownsort *et al.*, 2015; *Scottish Carbon Capture and Storage*, 2009; Akhurst *et al.*, 2011] was identified.

All four of these sandstone formations are important regional saline aquifers and have proven sealing and storage capacity in the form of major gas fields; for example, the South and North Morecambe fields in the Ormskirk Formation, East Irish Sea [Stuart and Cowan, 1991; Stuart, 1993; Meadows and Beach, 1993; Bastin *et al.*, 2003; Cowan and Boycott-Brown., 2003]; Esmond, Forbes, Gordon and Hewett fields in the Bunter Formation, Southern North Sea [Ketter, 1991a; Cooke-Yarborough, 1991; Cooke-Yarborough and Smith, 2003]; Ravenspurn, Leman and Viking fields in the Leman Formation, Southern North Sea [Ketter, 1991b; Hillier and Williams, 1991; Riches, 2003]; and Goldeneye, Blake, Cromarty and Captain fields in the Captain Sandstone Formation, Northern North Sea [Argent *et al.*, 2005]. The Leman Formation also contains two natural CO₂ accumulations, the Fizzy and Oak gas fields both of which contain 50-90% CO₂ [Pearce *et al.*, 1996; Underhill *et al.*, 2009], providing an analogue to CO₂ storage. Closed structures without gas charge, which provide structural traps for saline aquifer storage, have been identified in the Ormskirk Formation [Kirk, 2006] and Bunter Formation [Holloway *et al.*, 2006; Williams *et al.*, 2014; Noy *et al.*, 2012].

Estimates of the CO₂ storage capacity of these formations in both saline aquifers and depleted gas and oil fields in the Southern North Sea are 3.3 Gt CO₂ in the Leman Formation and up to 14.6 Gt CO₂ in the Bunter Formation [Holloway *et al.*, 2006]. Estimates of capacity in the Northern North Sea are up to 1.67 Gt CO₂ in the Captain Sandstone [Scottish Carbon Capture and Storage, 2009; Akhurst *et al.*, 2011, 2015; Jin *et al.*, 2012].

In March 2013, two projects were awarded funding under the UK Department of Energy and Climate Change (DECC) CCS Commercialisation Competition [Department of Energy and Climate Change, 2013]. Both projects involved capturing CO₂ at a major point

Sample	Porosity, ϕ	K_{abs} [D]	L [m]	$P_{c,entry}$ [Pa]
Bunter	0.260	2.2 ± 0.113	0.151	1964
Ormskirk	0.271	12.1 ± 0.787	.127	1097
Captain	0.267	$1.145 \pm .098$.235	1862

Table 2. Routine petrophysical properties of the samples

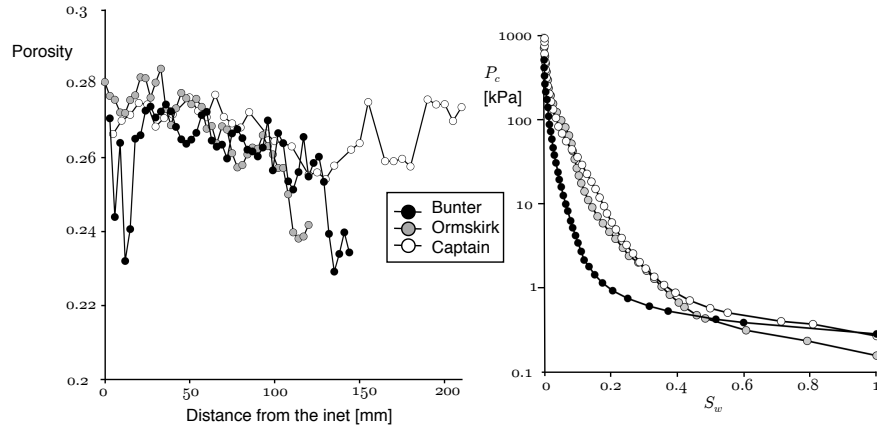


Figure 2. Porosity and capillary pressure characteristics of the samples

source and storing the CO₂ in a sandstone reservoir - Shell's Peterhead Project [Shell UK Limited, 2013] in the depleted Goldeneye gas field and Captain Sandstone saline aquifer and Capture Power's White Rose Project [Capture Power, 2013] in the Bunter Sandstone, Southern North Sea. These projects have now been cancelled after the removal of funding from the competition in November 2015 [Department of Energy and Climate Change, 2015; Shell UK Limited, 2015; White Rose Project, 2015]. However, storage in the Captain Sandstone saline aquifer and the depleted Goldeneye gas Field are the subject of a number of modelling studies and provide an example site for many site selection methodologies [Akhurst et al., 2015; Delprat-Jannaud et al., 2015; ScottishPower CCS Consortium, 2011a; Scottish Carbon Capture and Storage, 2011b]. Potential CO₂ storage sites in the Central and Northern North Sea are the best understood in the UK [Brownsort et al., 2016] but there are no published and peer-reviewed relative permeability or trapping curves. Consequently, three formations were selected for this study, the Bunter and Ormskirk Sandstones of the Sherwood Sandstone Group, and the Captain Sandstone.

2.2 Routine petrophysical properties

A routine rock characterisation was performed on the samples with data provided in Table 2. Absolute permeability was measured with experimental brine at experimental conditions using a standard method described in previous work by the authors [Reynolds and Krevor, 2015]. Mercury intrusion capillary pressure characteristic curves were measured using a Micromeritics Autopore IV 9500 Porosimeter and converted for CO₂ using the standard correction for interfacial tension (Figure 2). Thin section photos are shown in Figure 3 and brief rock descriptions are provided in the following. All four samples were classified as quartz arenites using the Folk classification scheme [Folk, 1957]. Grain size was assessed following Wentworth [1922] and roundness following Pettijohn et al. [2012].

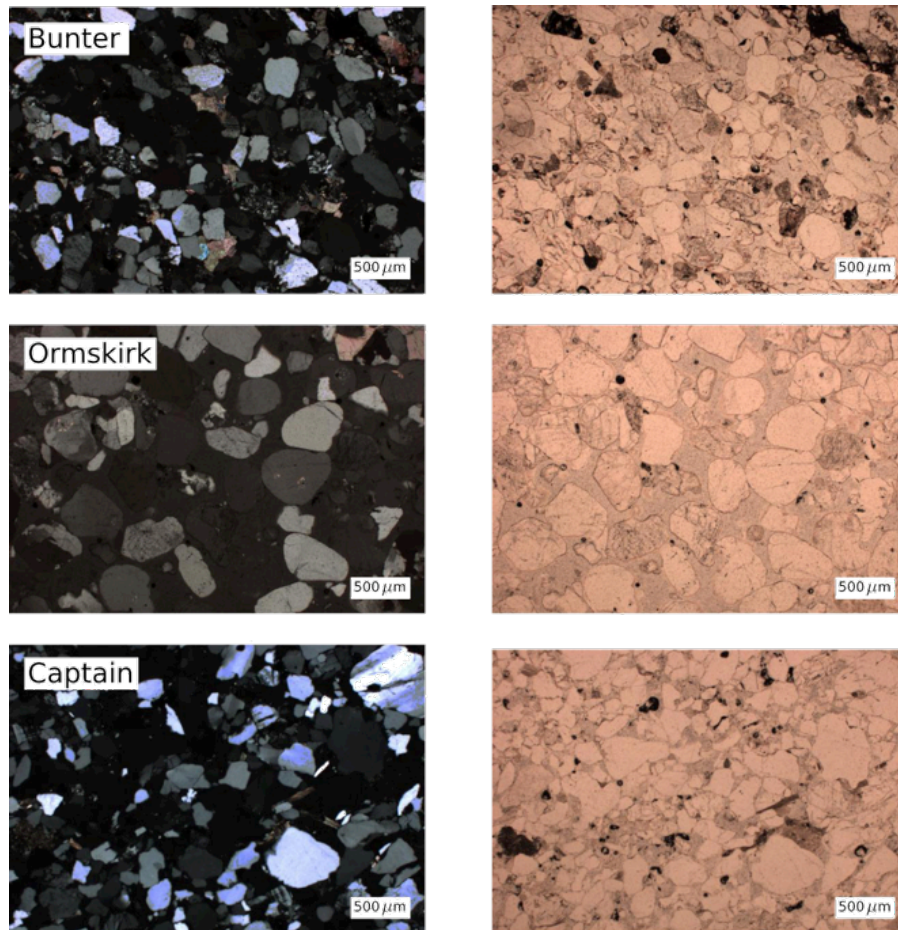


Figure 3. Photo micrographs of thin sections in cross (left) and plain (right) polarized light.

The Bunter Sandstone core had a porosity of 0.26 and a measured absolute permeability to brine of 2.2 D. This is a higher permeability than the core plug average from the Gordon, Esmond and Forbes ($K \approx 400$ mD, $\phi \approx 0.2$) fields but matches well with the porosity-permeability trend of measured core plugs [Noy *et al.*, 2012]. The Bunter Formation is a medium-grained sandstone composed mainly of sub-angular to sub-rounded quartz grains with a minor component of detrital K-feldspar, clay and carbonate clasts (Figure 3). Some altered quartz and K-feldspar overgrowths are present, as well as an intergranular cement mainly composed of dolomite [Hall *et al.*, 2015].

The Ormskirk Sandstone core had a porosity of 0.27, which was at the upper range of plug values typical of the South and North Morecambe field [Meadows and Beach, 1993]. The core sample had an extremely high permeability of 12 D, well in excess of the measured range of 0.0001 to > 1 D [Meadows and Beach, 1993]. The Ormskirk Formation is a medium-grained, mature sandstone predominantly composed of sub-rounded to rounded quartz grains. The presence or absence of illite as a pore lining cement is a major influence on the permeability of this formation [Kirk, 2006; Stuart, 1993]. However, no illite was observed in thin section (Figure 3) and the particular sample used for core-floods contained only dolomite and quartz cements. Absolute permeability was measured with a confining pressure of 5 MPa, which did not reflect the stress state present in the reservoir. It is possible that the measured absolute permeability would have been closer to the field average if performed with a higher confining pressure.

The Captain Sandstone core had a permeability of 1.1 D and porosity of 0.27, similar to samples from the Goldeneye field [McDermott *et al.*, 2016; Hangx *et al.*, 2013]. Much of the Captain Sandstone Formation is poorly consolidated and in the Captain Field permeabilities over 7 D are not uncommon [Rose, 1999; Lach, 1997]. However, a more consolidated and hence lower permeability core sample was obtained due to the difficulties of drilling core from poorly consolidated sandstone. The core was dominated by fine to medium-grained, angular to sub-angular quartz ($> 90\%$) with a minor feldspar component and some authigenic clay and intergranular cements of quartz, kaolinite and calcite [Hangx *et al.*, 2013].

3 Experimental methods

3.1 Relative permeability and capillary trapping

Two sets of drainage and imbibition relative permeability corefloods were performed on each core (Table 3). Tests were performed at high and low flow rates, following the approach of Reynolds and Krevor (2015) [Reynolds and Krevor, 2015], as observations at multiple rates allowed for an evaluation of the impacts of rock heterogeneity on flow, described in detail in Section 3.2. Where significant, capillary end effects were corrected for using an automated 1D numerical history match of the experiments, matching saturation and pressure observations. The flow rates were selected based on the heterogeneity and permeability of the rock cores. All the cores had observable heterogeneity in porosity and high absolute permeability (> 1 D) and a flow rate of 20 ml min^{-1} was used for the high flow rate observations. The lower flow rate experiments were performed with flow rates in the range of $0.2 - 4 \text{ ml min}^{-1}$. This range of flow rates was the practical range that could be achieved safely with our experimental setup. The low end of the range resulted in flow velocities overlapping with the upper range of rates expected to prevail in the reservoir system, while the upper end of the range far exceeded velocities anticipated anywhere greater than a metre from an injection point [Blunt, 2017].

Residual trapping was characterised in separate core flood tests, following the procedure described in Niu *et al.* (2015) [Niu *et al.*, 2015]. In these tests drainage flow rates were chosen to establish the initial saturation. Higher flow rates generally lead to higher initial saturations. Imbibition was performed at low flow rates for consistency with the trapping process in the reservoir.

Sample	Temp. [°C]	Pressure [MPa]	Salinity [mol kg ⁻¹]	Number	Type	Total flow rate [ml min ⁻¹]
Bunter	53	13.1	1	B1	Drainage	20
				B2	Imbibition	20
				B3	Drainage	20
				B4	Imbibition	20
				B5	Drainage	0.2
				B6	Imbibition	0.2
				B7	Trapping	20/0.5
				B8	Trapping	0.5/0.5
Ormskirk	33	12.7	4.32	O1	Drainage	20
				O2	Imbibition	20
				O3	Drainage	4
				O4	Imbibition	4
				O5	Trapping	20/2
				O6	Trapping	1.5/1.5
Captain	80	18	1	C1	Drainage	20
				C2	Imbibition	20
				C3	Drainage	2
				C4	Imbibition	2
				C5	Trapping	20/2

Table 3. Experimental conditions of the relative permeability and residual trapping tests

Pressure, temperature and salinity conditions were chosen so as to be representative of likely injection sites in each formation, either by using site specific conditions or regional averages for the formation (Table 3). Pressure and temperature for the Bunter sandstone were taken from the Hewett field and a regional average salinity for Bunter Formation reservoir brines in the Southern North Sea was used [Williams *et al.*, 2014; Noy *et al.*, 2012; Downing and Gray, 1986]. The conditions of the South and North Morecambe fields were used for the Ormskirk sandstone rock core [Stuart and Cowan, 1991; Cowan and Boycott-Brown., 2003]. Pressure and temperature for the Goldeneye field and regional Captain Sandstone brine salinities were used for the Captain sandstone sample [Jin *et al.*, 2012; Scottish Carbon Capture and Storage, 2011b; Hangx *et al.*, 2013].

3.2 Characterising capillary pressure characteristic heterogeneity

X-ray computed tomography scans were used to create three-dimensional images of saturation, which formed the observational basis for the characterisation of capillary pressure characteristic heterogeneity [Pini and Benson, 2013b; Pini *et al.*, 2012; Krause *et al.*, 2013; Egermann and Lenormand, 2005]. Capillary pressure characteristic curves obtained from mercury porosimetry observations (Figure 2) were assumed to represent an upscaled curve, representative of the whole core. The capillary pressure at the inlet face of the rock core was controlled by the boundary conditions of the core flood [Ramakrishnan and Cappiello, 1991]. It was assumed that the capillary pressure was also constant for a given slice, or location along the principal axis, of the rock core [Krause *et al.*, 2013]. Variations in saturation within a slice were then assumed to be due to variations in the capillary pressure characteristic function [Egermann and Lenormand, 2005]. Assuming that the form of the curve was the same throughout the rock core, e.g., that *J*-scaling applied, heterogeneity was described quantitatively by the degree of scaling required between the average capillary pressure function and the particular function of a given location [Pini and Benson, 2013b].

In this work we followed the approach of *Pini and Benson, 2013* [Pini and Benson, 2013b] in using a simple “vertical” scaling, relating local functions to the average through a linear shifting of the capillary entry pressure,

$$P_c(x, y, z, S_w) = \kappa(x, y, z)P_{c,a}(S_w). \quad (1)$$

Here $P_c(x, y, z, S_w)$ was the capillary pressure characteristic function for a given location. It was related to the average function, $P_{c,a}(S_w)$, through the location specific dimensionless scaling parameter κ .

To obtain the value of κ for each location, first the slice averaged saturation was used to obtain the capillary pressure at each fractional flow of the experiment and thus generate local capillary pressure curves. The core representative capillary pressure curve (in this case obtained from mercury porosimetry) was then scaled using Equation 1 in a regression algorithm varying κ until a best fit was obtained with the data for a given location.

The capillary pressure heterogeneity in the rock core was characterised using a best-fit spatial map of the scaling parameter κ . Although the assumption of constant capillary pressure within a slice is only valid at the inlet boundary of the rock core, this data can be used as a first guess in an iterative approach to generating an accurate heterogeneous numerical model of the core, using the local variation in the capillary pressure function [Krause *et al.*, 2013]. This type of data has also been used in the generation of statistical realisations of rock core models [Kong *et al.*, 2015].

The relative importance of capillary driven flow, i.e., the role of capillary heterogeneity relative to permeability heterogeneity, is characterised through a dimensionless capillary number describing the ratio of viscous or buoyantly driven flow to flow driven by gradients in capillary pressure [Yokoyama and Lake, 1981; Zhou *et al.*, 1997; Virnovsky *et al.*, 2004; Jonoud and Jackson, 2008; Kuo and Benson, 2015]. We used the number defined by Virnovsky *et al.* (2004) [Virnovsky *et al.*, 2004] due to its simplicity and correspondence with observables in our experiments.

The capillary number is defined as,

$$N_c = \frac{\Delta P}{L} \frac{H}{\Delta P_c}, \quad (2)$$

where ΔP [kPa] is the pressure differential measured between the inlet and outlet face of the rock core during flooding, L [m] is the length of the rock core, H [m] is a characteristic distance between layers, and ΔP_c [kPa] is a characteristic difference in capillary pressure between layers. The characteristic difference in capillary pressure, ΔP_c , was taken to be a single standard deviation in the distribution of entry pressure obtained through scaling the average capillary pressure function, Equation 1. The characteristic lengthscale for heterogeneity, H , was obtained by inspection of the three-dimensional map of the scaling parameter κ .

At larger capillary numbers, the impact of the capillary pressure characteristic heterogeneity becomes less dominant. A number of studies have shown that a universal scaling number cannot be derived, in part due to the dependence of the impact on the spatial structure of the heterogeneity [Jonoud and Jackson, 2008; Pickup and Stephen, 2000]. Virnovsky *et al.* (2004) [Virnovsky *et al.*, 2004] suggested that a transition between capillary and viscous dominated flows might take place in the range of capillary number $1 < N_c < 100$, which has been confirmed experimentally by Reynolds and Krevor (2015) [Reynolds and Krevor, 2015].

4 Results

4.1 Heterogeneity in the rock samples

Three-dimensional maps and individual slices of the capillary pressure characteristic scaling parameter, κ (Equation 1), are shown in Figure 4. Faults with the X-ray scanner affected three slices of the Captain sandstone sample, and those slices are absent in the figure. Millimetre-scale bedding was visible in all three of the rocks, but most prominently in the Bunter and Ormskirk sandstones, while the Captain sandstone had large homogeneous regions without bedding. Using individual slices to assess the bedding structure, we find the characteristic length scale of all of the rocks to be $H \approx 1$ cm (Equation 2).

The strength and degree of heterogeneity in the capillary pressure characteristic functions was apparent from the frequency distribution of the best fit entry pressures (Figure 5, with $P_{c,\text{entry}} = \kappa P_{c,a,\text{entry}}$ from Equation 1). The Bunter sandstone had the greatest mean entry pressure of 1.8 kPa and the most widely distributed entry pressures, with a standard deviation of 0.4 kPa. The Captain sandstone had a mean entry pressure of 0.32 kPa and a standard deviation of 0.17 kPa. The Ormskirk sandstone had a narrow distribution with a mean entry pressure of 0.11 kPa and standard deviation of 0.027 kPa.

4.2 The Bunter Sandstone

Two sets of high flow rate and one set of low flow rate drainage and imbibition relative permeability tests were performed. At high flow rates (Experiments B1-4) the highest relative permeability to CO₂, $0.1 \leq k_{r,\text{CO}_2} \leq 0.12$, was obtained in the saturation range $0.27 \leq S_w \leq 0.32$ (tabular values are provided Table A.2 of A:). Measurements of relative permeability here and elsewhere show that reported observations of a low maxima in the observed relative permeability to CO₂ are not a result of a weakened wetting, but due to the limitations of the experimental apparatus used [Krevor *et al.*, 2012; Akbarabadi and Piri, 2013; Pini and Benson, 2013a; Manceau *et al.*, 2015]. The water relative permeability decreased sharply with decreasing water saturation and the cross point was shifted to lower water saturations ($S_w = 0.5$) compared with the low flow-rate core-floods. There was a slight hysteresis in the k_{r,CO_2} curves, with the imbibition permeability higher than the drainage permeability. This was a manifestation of the role that rock heterogeneity had in the measurement, even at the high flow rate, and is discussed further below. As is typical for water wetting rocks, there was no discernible hysteresis in the water relative permeability curves.

For the low flow rate observations, B5 and B6, the highest k_{r,CO_2} was low, $O(10^{-3})$. The k_{r,CO_2} was lower for imbibition than for drainage, the opposite of what was observed in the high flow rate observations. There was also significant hysteresis in the $k_{r,w}$ curves. The permeability during imbibition was significantly higher than during drainage. These differences highlight how the impact of rock heterogeneity emerged at lower capillary numbers.

The varying impact of rock heterogeneity was evaluated by inspecting the distribution of fluid saturation at a location within the rock core at a range of average saturations and capillary numbers, Figure 7 (tabular values of the measured pressure differential used in the calculation of N_c are provided in A:). In the high flow rate observations (B3 and B4 in Figure 7) the observations were made across a wide range of capillary number. Capillary numbers were initially high at the beginning of the drainage process with a high water fractional flow and the fluid was homogeneously distributed when $N_c > 5$. As the CO₂ fractional flow was increased, the capillary number decreased, primarily due to the lower viscosity of CO₂, but also because the relative permeability to CO₂ was increasing with increasing CO₂ saturation. The impact of heterogeneity emerged at the low capillary numbers, and could be observed in the saturation maps at the end of drainage and the beginning of imbibition. At the end of imbibition, when the capillary number increased again beyond $N_c > 5$, the homogenous fluid distribution was re-established. The capillary number was low throughout the low flow rate

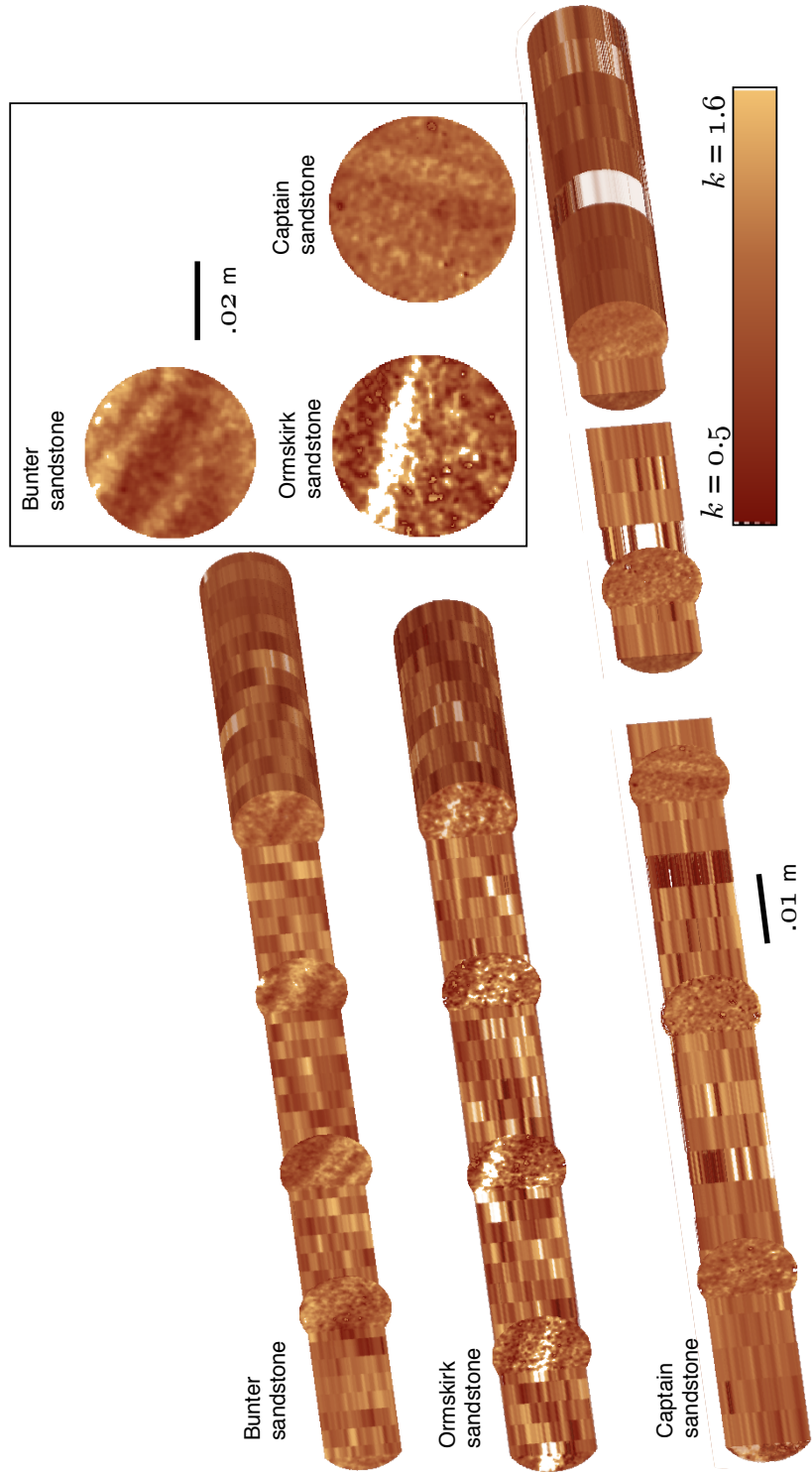


Figure 4. The distribution of κ (Equation 1) for the three rock samples. There were faults with the X-ray scanner affecting three slices of the Captain sandstone sample, and those slices are absent in the figure

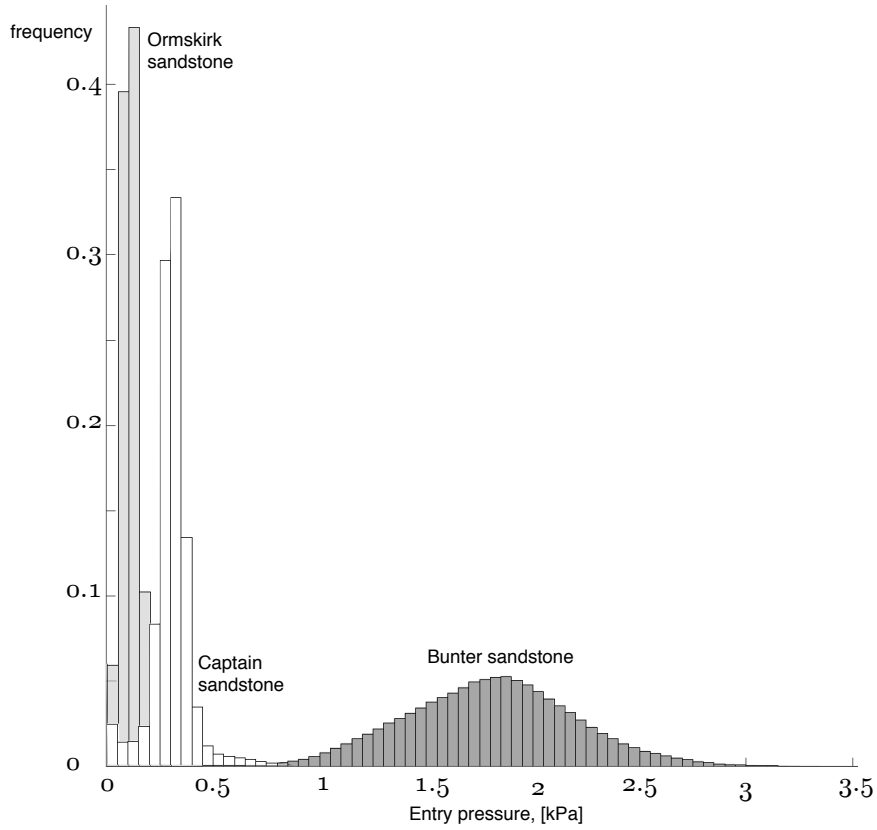


Figure 5. Frequency histograms showing the distribution of the best fit entry pressures for the three rocks analysed in the study. One standard deviation in the distributions were used to calculate the capillary numbers.

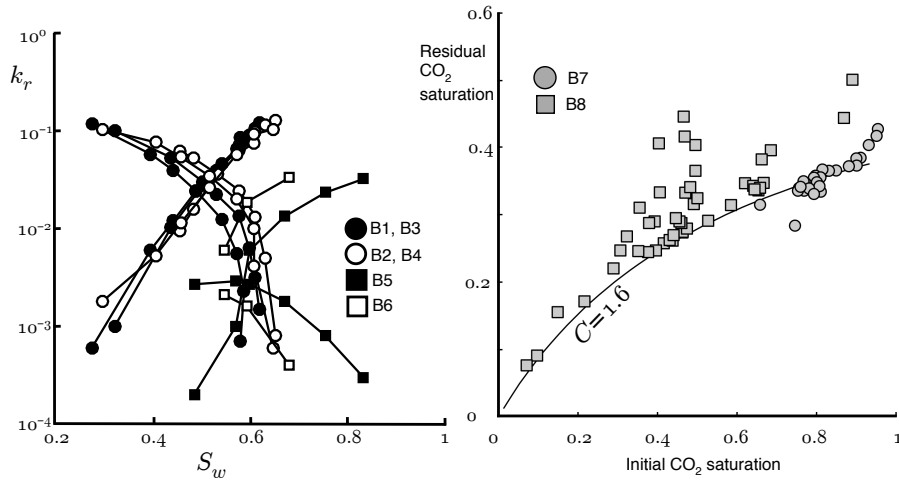


Figure 6. Relative permeability and residual trapping characteristic curves for the Bunter Sandstone sample measured during drainage and imbibition at two capillary numbers. Drainage is shown with filled symbols and imbibition is shown with unfilled symbols. The high capillary number observations are represented with circles and the low capillary number observations are represented with squares. The curve on the residual trapping graph is the Land model with the labeled coefficient.

observations (B5 and B6) and the layering of the rock was evident in all cases with capillary numbers well below $N_c < 5$.

For the two sets of drainage and imbibition tests the main impact of the heterogeneity was to significantly decrease the observed relative permeability at low flow rate (B5 and B6 relative to B1-B4 in Figure 6). The other clear impact was in the varying nature of the hysteresis. The heterogeneity in the high flow rate observations resulted in a higher imbibition than drainage relative permeability, whereas the opposite was observed in the low flow rate tests. At low flow rate, however, the increased role of heterogeneity resulted in significant hysteresis in both wetting and non-wetting phase relative permeability curves.

Residual trapping experiments (Experiments B7 and B8) showed a range of residually trapped CO₂ saturations from $0.3 < S_{\text{CO}_2} < 0.6$ for initial CO₂ saturations of $S_{\text{CO}_2} > 0.8$. A lower bound on the trapping was characterised by a Land coefficient of $C = 1.6$, although a subset of the trapped fluid fell well above the saturation predicted by the Land Model. This was due to the trapping of fluid behind local capillary heterogeneities and is distinct from the primarily pore scale phenomenon of capillary trapping [Saadatpoor *et al.*, 2009; Krevor *et al.*, 2011, 2015].

4.3 The Ormskirk Sandstone

Both high and low flow rate drainage tests resulted in similarly shaped relative permeability curves (Figure 8) which showed a sharp increase in k_{r,CO_2} and a sharp decrease in $k_{r,w}$ with decreasing S_w . The cross points for both curves were at $S_w > 0.5$ indicating that the Ormskirk sandstone was water wetting. Higher CO₂ saturation ($S_w = 0.27$) and a corresponding CO₂ relative permeability close to unity were achieved during the high flow rate observations. The low flow rate observations resulted in curves shifted to the right, with higher k_{r,CO_2} for a given saturation but lower $k_{r,w}$. The maximum relative permeability to CO₂ was $k_{r,\text{CO}_2} = 0.1$ at $S_w = 0.72$, with the low flow rate having limited the achievable capillary pressure.

The shift in the curves with flow rate contrasted with the results for the Bunter core, where the relative permeability to both fluids were higher in the high flow rate case. The difference was likely due to the orientation of the heterogeneity in the core with respect to the principal flow direction and radial boundaries. There was little hysteresis between drainage and imbibition for the viscous dominated experiments, and Experiment O1 had a very similar shape to Experiment O2. In the low flow rate experiments (O3 and O4) the imbibition k_{r,CO_2} showed classic hysteresis behaviour, where the relative permeability dropped rapidly with increasing water saturation and was orders of magnitude lower at a given saturation during imbibition compared to drainage. However, similar to the Bunter Sandstone, the $k_{r,w}$ was higher for imbibition than for drainage.

The impact of heterogeneity on flow is shown in Figure 9. As with the Bunter sandstone, the impact of rock heterogeneity emerged at lower capillary number and was not apparently sensitive the average saturation (vertical axis in Figure 9). The threshold capillary number for this sample was $N_c \approx 30$, with layering apparent in all of the imagery from observations at lower capillary numbers.

There was a wide range in residual trapping behaviour for the Ormskirk core (Figure 8) - the Land trapping model was not a good descriptor of trapping, and coefficients encompassing the data varied from $C = 0.05$ ($S_r \approx S_i$) to $C = 3$ ($S_r < S_i/2$). This was due to rock heterogeneity and suggests that the residual CO₂ saturation achievable in this formation was highly dependent on the contrast in capillarity between homogeneous layers.

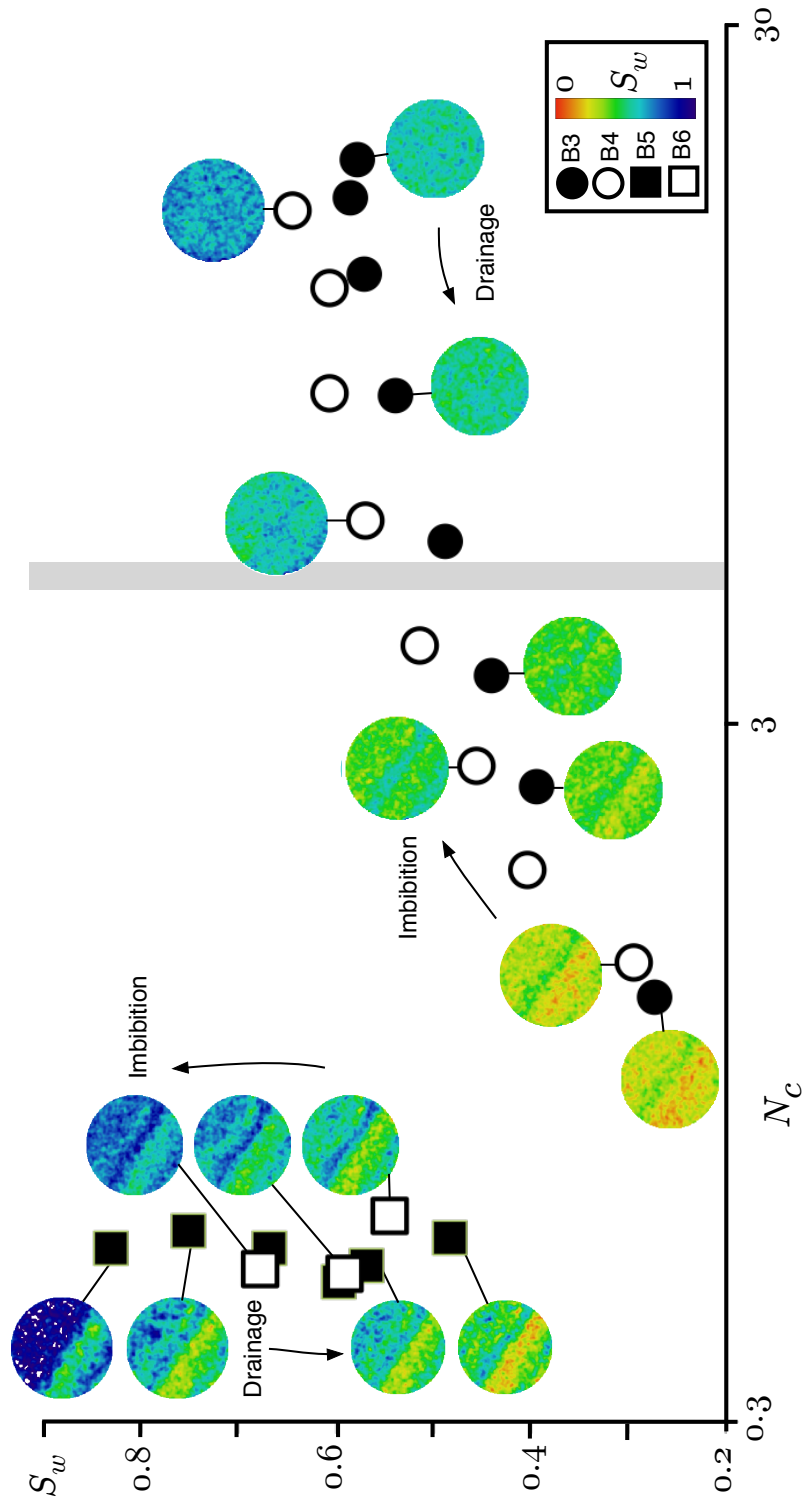


Figure 7. Capillary number vs water saturation and corresponding slice saturation maps for the Bunter sandstone. The slice shown was at the same location for all four sets of observations. The vertical grey bar shows the approximate location where the viscous limit was achieved.

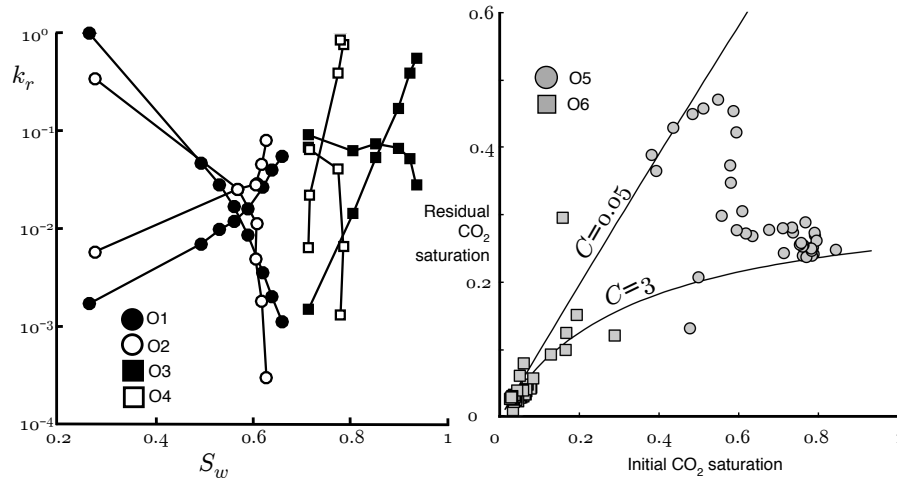


Figure 8. Relative permeability and residual trapping characteristic curves for the Ormskirk Sandstone sample measured during drainage and imbibition at two separate flow rates. Drainage is shown with filled symbols and imbibition is shown with unfilled symbols. The high capillary number observations are represented with circles and the low capillary number observations are represented with squares. Curves on the residual trapping graph are the Land model with the labeled coefficients.

4.4 The Captain sandstone

The shape of the drainage relative permeability curves was similar for the high (C1) and low (C3) flow rate experiments, indicative of a water wetting system. The $k_{r,w}$ and k_{r,CO_2} were shifted towards the right, with generally lower $k_{r,w}$ and higher k_{r,CO_2} at a given saturation, although the k_{r,CO_2} was lower at lower S_w in the high flow rate case (Figure 10). The highest relative permeability to CO_2 , $k_{r,CO_2} = 0.46$ was achieved at $S_w = 0.34$ during the high flow rate experiment. At the low flow rate, $k_{r,CO_2} = 0.02$ was obtained for $S_w = 0.60$. Imbibition k_{r,CO_2} showed classic hysteresis behaviour at low flow rate, but was higher than the drainage k_{r,CO_2} during the high flow rate observations. Additionally, $k_{r,w}$ was higher for imbibition than drainage for both low and high flow rate experiments. This again suggested that rock heterogeneity had a significant impact on the observed permeability, even at the highest flow rates used in these observations.

As with the Bunter and Ormskirk sandstones, the impact of heterogeneity on flow became apparent in observations of the fluid distribution at low capillary numbers (Figure 11). The layering in the rock was apparent in all of the imagery obtained when $N_c < 20$. This was observed in both low and high flow rate observations, during both drainage and imbibition, and across a saturation range $0.2 < S_w < 1$.

A single residual trapping experiment was performed (Experiment C5), for which trapping was scattered between Land models with coefficient $0.8 < C < 3$. The significant scatter was indicative of the role that capillary heterogeneity was playing in controlling the residually trapped CO_2 .

5 Discussion and Conclusions

The fundamental attribute of the observations was that centimetre scale heterogeneity had a strong impact on drainage and imbibition relative permeability, as well as residual trapping. At this scale, the continuum or Darcy theory of multiphase flow suggests that capillary pressure characteristic heterogeneity impacts flow far more than permeability or

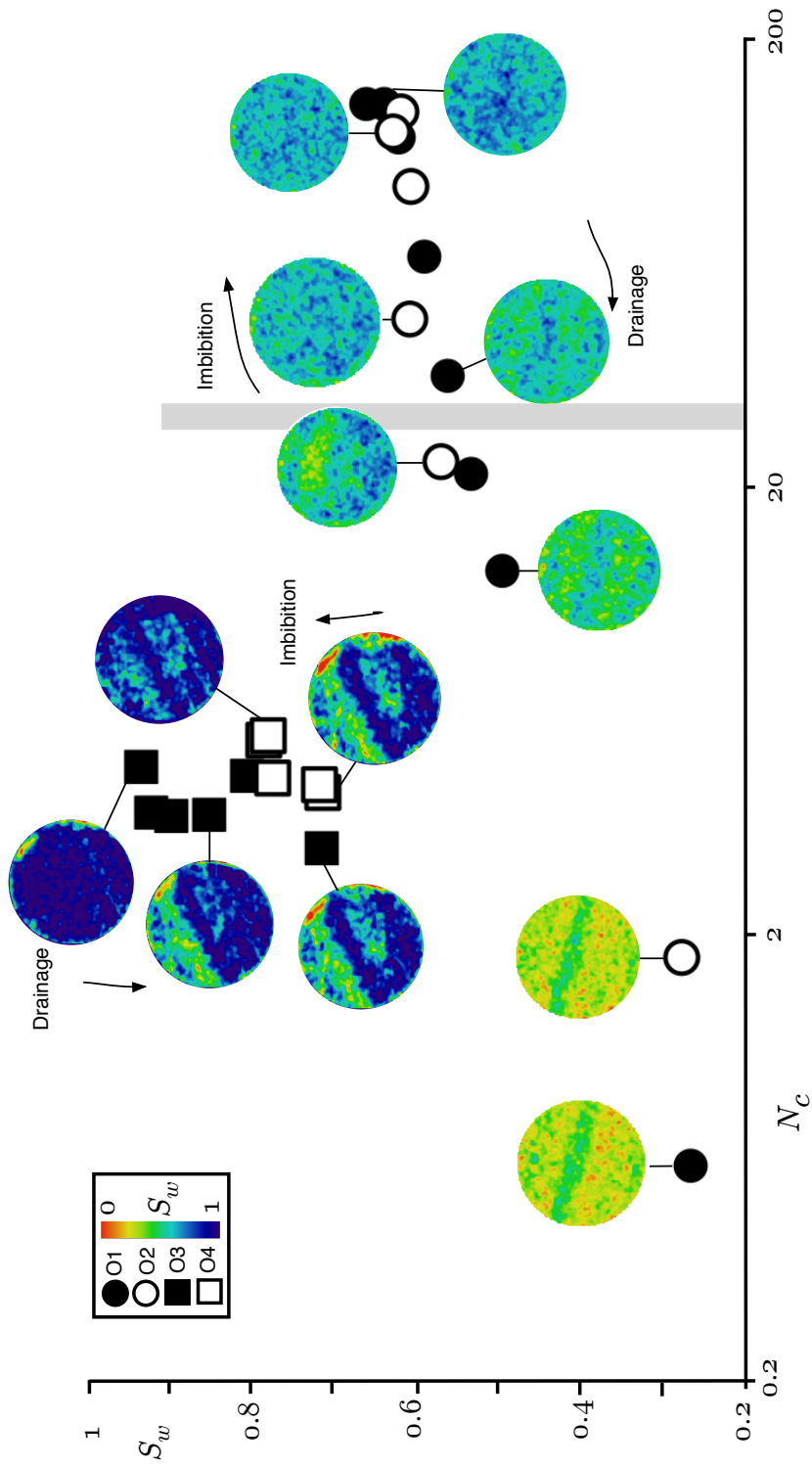


Figure 9. Capillary number vs water saturation and corresponding slice saturation maps for the Ormskirk sandstone. The slice shown was at the same location for all four sets of observations, but the orientation of the core varied between the high and low flow rate experiments. The vertical grey bar shows the approximate location where the viscous limit was achieved.

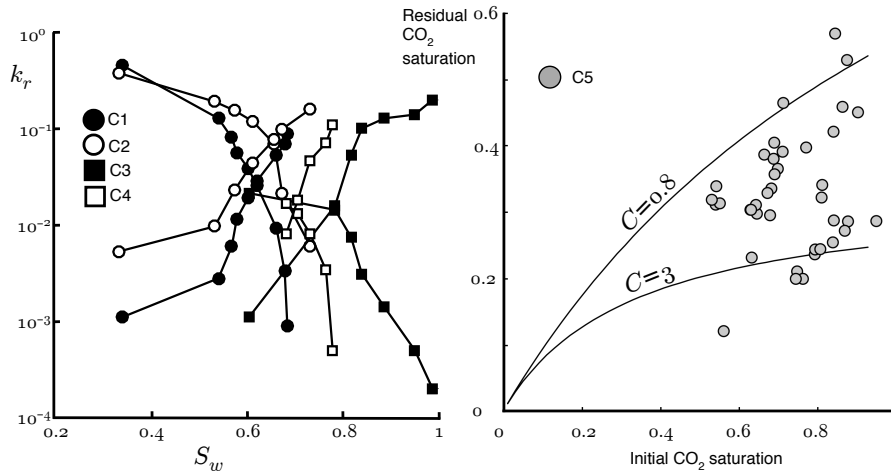


Figure 10. Relative permeability and residual trapping characteristic curves for the Captain Sandstone sample measured during drainage and imbibition at two separate capillary numbers. Drainage is shown with filled symbols and imbibition is shown with unfilled symbols. The high capillary number observations are represented with circles and the low capillary number observations are represented with squares. Curves on the residual trapping graph are the Land model with the labeled coefficients.

porosity heterogeneity [Zhou *et al.*, 1997]. This was supported by the utility of the continuum scale capillary number in identifying threshold conditions at which the heterogeneity became apparent. There was a range of threshold capillary number for the three rock samples, $5 < N_c < 30$. This has been anticipated in studies indicating that there cannot be a universal scaling group due to the dependence on the spatial organisation of the heterogeneity and the sample-specific nature of the relative permeability and capillary pressure characteristic curves [Jonoud and Jackson, 2008; Pickup and Stephen, 2000]. Numerical studies have suggested that a transition between capillary and viscous dominated flows might take place in the range of capillary number $1 < N_c < 100$, consistent with the observations reported here [Virnovsky *et al.*, 2004].

The hysteresis between drainage and imbibition, and the residual trapping characteristics were controlled by the heterogeneity in the rock cores, in addition to the conventionally considered pore scale trapping phenomena. At high flow rates, hysteresis was not always present in k_{r,CO_2} . In some experiments $k_{r,w}$ and k_{r,CO_2} were higher for drainage than for imbibition. Hysteresis behaviour is usually attributed to the particular pore space morphology, in particular the ratio between pore body diameter and pore throat diameter which promotes or restricts snap-off [Krevor *et al.*, 2015; Akbarabadi and Piri, 2013; Ruprecht *et al.*, 2014]. In this case, changes in the behaviour between flow rates reflects the varying impact of heterogeneity with the change in capillary-viscous force balance. Additionally, the residual trapping data for all three rocks diverged significantly from conventional trapping models, e.g., the Land trapping model. A significant fraction of the residually trapped CO_2 was immobilised behind local capillary heterogeneities. This has been observed experimentally [Krevor *et al.*, 2011] and modelled [Debbabi *et al.*, 2016; Meckel *et al.*, 2015], and in some reservoirs may be a more significant source of fluid trapping than the pore-scale trapping.

More generally, the observations here show that small scale rock heterogeneity has a large impact on the key flow attributes used in reservoir simulation, the relative permeability, hysteresis, and residual trapping. The effects are dependent on the strength and orientation of the heterogeneity in addition to the prevailing flow regime. It is unlikely that they would be predicted in advance of laboratory measurements, and using data obtained with conventional

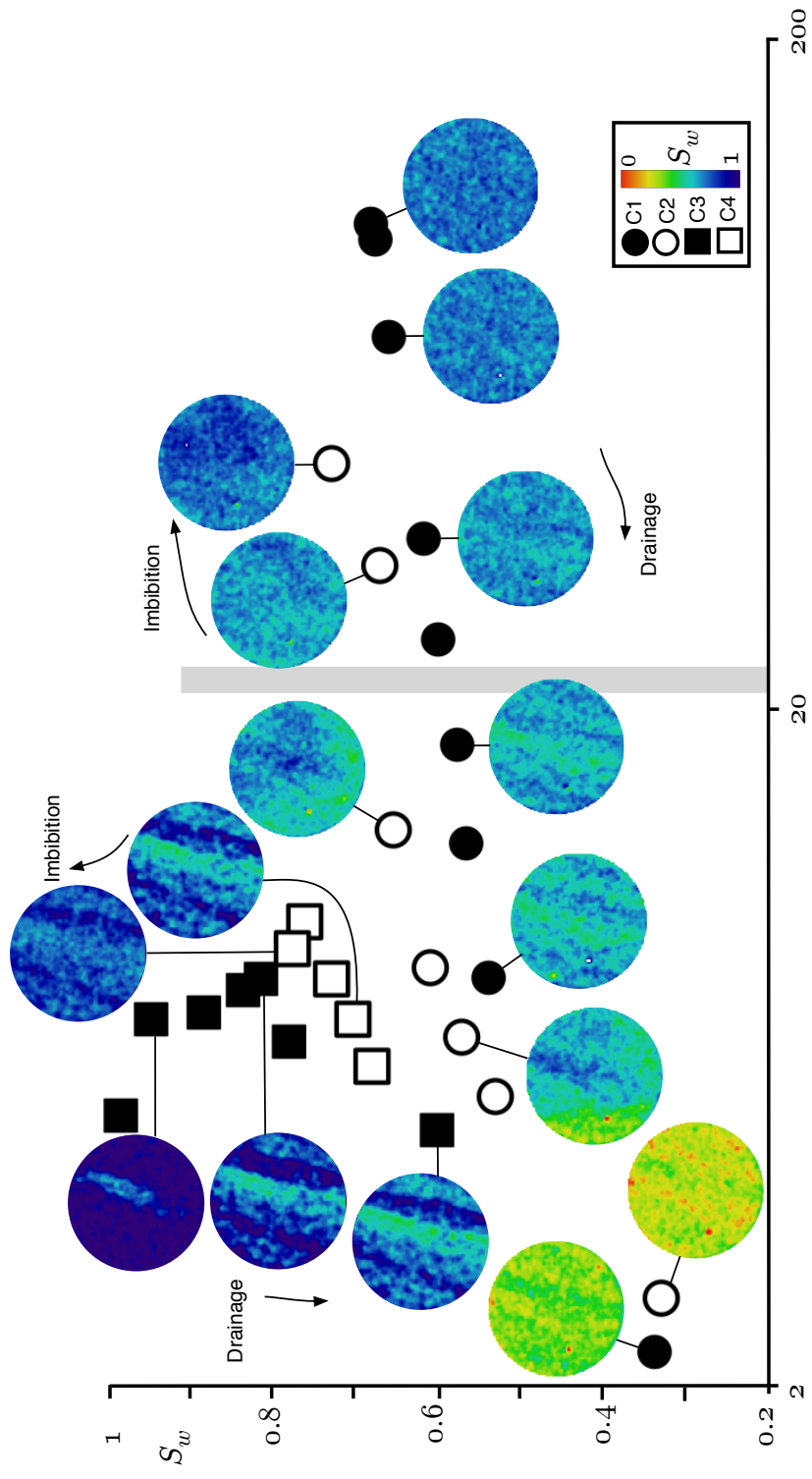


Figure 11. Capillary number vs water saturation and corresponding slice saturation maps for the Captain sandstone. The slice shown was at the same location for all four sets of observations. The vertical grey bar shows the approximate location where the viscous limit was achieved.

Experiment	f_{CO_2}	S_w	k_{r,CO_2}	$k_{r,w}$	ΔP [kPa]
B1	0.8904	0.6168	0.0015	0.1213	89.04
	0.8432	0.6079	0.0032	0.1069	84.32
	0.7268	0.5963	0.0063	0.0919	72.68
	0.5293	0.5758	0.0134	0.0648	52.93
	0.3801	0.5281	0.0227	0.0394	38.01
	0.2985	0.5004	0.0307	0.0278	29.85
	0.1794	0.436	0.0539	0.0103	17.94
	0.0967	0.3202	0.1015	0.001	9.669
B2	0.9883	0.453	0.0628	0.0095	15.44
	0.9768	0.4822	0.0531	0.016	18.05
	0.9262	0.5302	0.0365	0.0369	24.88
	0.814	0.5761	0.0247	0.0716	32.34
	0.6277	0.609	0.0133	0.1003	46.23
	0.3575	0.6283	0.005	0.1148	69.71
	0.0762	0.6503	0.0008	0.1285	89.51
	B3	0.0926	0.5782	0.0007	0.0861
0.2662		0.5858	0.0023	0.0789	102.1
0.5176		0.5711	0.0056	0.0667	79.37
0.7738		0.5397	0.0126	0.0466	53.27
0.9262		0.4875	0.0244	0.0246	32.91
0.9768		0.4401	0.04	0.012	21.15
0.9919		0.3942	0.0584	0.0061	14.69
0.9996		0.2731	0.118	0.0006	7.328
B4	0.9987	0.295	0.1052	0.0018	8.211
	0.9956	0.4038	0.0773	0.0053	11.14
	0.9834	0.4565	0.0541	0.0116	15.74
	0.9435	0.5147	0.0349	0.0266	23.37
	0.814	0.5703	0.02	0.0579	35.25
	0.6277	0.6062	0.0101	0.0763	53.57
	0.3575	0.6062	0.0041	0.0931	75.73
	0.0625	0.6445	0.0006	0.105	97.96

Table A.1. Tabular relative permeability data for the high flow rate experiments with the Bunter sandstone sample. See Table 3 for the corresponding experimental conditions.

workflows runs the risk of significantly over or under-prediction of flow and trapping in the reservoir system.

It is possible that these types of observations could be coupled with numerical simulation to overcome these challenges. The need to simulate flow in heterogeneous reservoir systems at larger scales has led to the development of numerical upscaling techniques which are widely used in industry [Rabinovich *et al.*, 2015; Ringrose and Bentley, 2015; Ringrose *et al.*, 1993; Corbett *et al.*, 1992]. Less well understood, however, is the best approach for characterising small scale heterogeneities in rock samples in the laboratory. The types of observations reported herein can be used in the construction of a core-scale digital rock model [Kong *et al.*, 2015; Krause *et al.*, 2013], which can form the basis for the initial stages in an upscaling workflow. Another benefit is that synthetic relative permeability curves could be generated quickly through simulation at many capillary numbers rather than attempting to measure multiple representative relative permeability curves covering the range of flow conditions relevant to the reservoir system. In principle, the orientation of the rock heterogeneity could also be restructured to evaluate flow independent of the impacts of the radial boundaries of the core flood.

A: Tabular relative permeability data

Acknowledgments

The research was performed as a part of the UKCCSRC Call 2 project Multiscale Characterisation of CO₂ storage reservoirs in the United Kingdom. The UKCCSRC is supported by the EPSRC as part of the Research Councils UK Energy Program. Catriona Reynolds received

Experiment	f_{CO_2}	S_w	k_{r,CO_2}	$k_{r,w}$	ΔP [kPa]
B5	0.1	0.8306	0.0003	0.0325	3.203
	0.31	0.7522	0.0008	0.0235	3.394
	0.63	0.6688	0.0018	0.0134	3.203
	0.85	0.597	0.0027	0.006	2.876
	0.975	0.5688	0.0029	0.001	3.027
	0.995	0.4833	0.0027	0.0002	3.318
B6	0.815	0.5453	0.0021	0.006	3.564
	0.52	0.5914	0.0016	0.0189	2.946
	0.135	0.6783	0.0004	0.0334	2.994

Table A.2. Tabular relative permeability data for the low flow rate experiments with the Bunter sandstone sample. See Table 3 for the corresponding experimental conditions.

Experiment	f_{CO_2}	S_w	k_{r,CO_2}	$k_{r,w}$	ΔP [kPa]
O1	0.2572	0.6622	0.0011	0.0543	48.24
	0.4611	0.6411	0.002	0.0394	48.2
	0.694	0.6231	0.0035	0.0265	40.75
	0.9003	0.592	0.0085	0.016	22.02
	0.9596	0.5637	0.0166	0.0119	11.97
	0.9802	0.5342	0.0281	0.0097	7.228
	0.9913	0.4966	0.0468	0.007	4.394
	0.9999	0.2669	0.9963	0.0017	0.208
	O2	0.999	0.2788	0.3417	0.0058
0.9443		0.5716	0.0254	0.0254	7.713
0.8705		0.6095	0.0113	0.0285	16.04
0.7461		0.6073	0.0049	0.0283	31.57
0.4044		0.6204	0.0018	0.0453	46.37
0.059		0.6298	0.0003	0.0792	41.85
O3	0.461	0.9365	0.0277	0.5497	1.604
	0.694	0.9235	0.0526	0.3942	1.27
	0.8705	0.8995	0.067	0.1695	1.25
	0.9595	0.8536	0.0737	0.0528	1.254
	0.9868	0.8068	0.062	0.0141	1.532
	0.999	0.7162	0.0906	0.0015	1.061
O4	0.9945	0.7156	0.0681	0.0064	1.406
	0.9803	0.7187	0.0641	0.022	1.471
	0.638	0.7768	0.0405	0.3907	1.516
	0.1275	0.7872	0.0066	0.772	1.849
	0.026	0.7815	0.0013	0.8425	1.891

Table A.3. Tabular relative permeability data for the Ormskirk sandstone sample. See Table 3 for the corresponding experimental conditions.

Experiment	f_{CO_2}	S_w	k_{r,CO_2}	$k_{r,w}$	ΔP [kPa]
C1	0.0954	0.6828	0.0009	0.0879	419.3
	0.3171	0.6772	0.0033	0.0701	396.8
	0.6294	0.6604	0.0092	0.053	284.6
	0.8991	0.619	0.026	0.0286	143.6
	0.9521	0.6014	0.0388	0.0192	101.8
	0.9797	0.5776	0.057	0.0116	71.26
	0.9926	0.5672	0.081	0.006	50.81
	0.9978	0.5395	0.1284	0.0028	32.21
	0.9998	0.3388	0.4599	0.0011	9.016
C2	0.9986	0.3314	0.3822	0.0053	10.83
	0.9949	0.5319	0.1918	0.0097	21.51
	0.9852	0.5727	0.1554	0.0229	26.29
	0.9635	0.6107	0.1199	0.0446	33.31
	0.8991	0.6552	0.0701	0.0773	53.19
	0.68	0.6719	0.0215	0.0995	131.1
	0.2731	0.7299	0.0061	0.1597	185.4
C3	0.01	0.9846	0.0002	0.2002	20.15
	0.0335	0.9478	0.0005	0.1409	27.94
	0.0955	0.8848	0.0014	0.1288	28.61
	0.2335	0.8378	0.0031	0.101	30.92
	0.5765	0.8152	0.0075	0.0538	32.05
	0.899	0.782	0.0144	0.0159	25.95
	0.995	0.6028	0.0215	0.0011	19.15
C4	0.952	0.6807	0.0166	0.0082	23.8
	0.874	0.7048	0.013	0.0184	27.94
	0.6295	0.7297	0.0082	0.0471	32.03
	0.317	0.7632	0.0034	0.0714	38.96
	0.042	0.777	0.0005	0.1097	35.59

Table A.4. Tabular relative permeability data for the Captain sandstone sample. See Table 3 for the corresponding experimental conditions.

funding through the EPSRC Doctoral Training Programme Grant 1304506. The research was performed in the laboratories of the Qatar Carbonates and Carbon Storage Research Centre at Imperial College London. Data associated with this work may be obtained by contacting s.krevor@imperial.ac.uk

References

- Akbarabadi, M., and M. Piri (2013), Relative permeability hysteresis and permanent capillary trapping characteristics of supercritical CO₂/brine systems: an experimental study at reservoir conditions, *Advances in Water Resources*, 52, 190–206.
- Akhurst, M., S. D. Hannis, M. F. Quinn, J.-Q. Shi, M. Koenen, F. Delprat-Jannaud, J.-C. Lecomte, D. Bossie-Codreanu, S. Nagy, and L. Klimkowski (2015), Risk assessment-led characterisation of the SITECHAR UK North Sea site for the geological storage of CO₂, *Oil & Gas Science and Technology-Revue d'IFP Energies nouvelles*, 70(4), 567–586.
- Akhurst, M. C., J. D. L. Gaera, K. Hitchen, T. Kearsley, D. J. D. Lawrence, D. Long, M. McCormac, M. F. Quinn, R. Catterson, J. M. Farley, A. Young, J. Veenboer, M. Jin, E. Mackay, A. E. Todd, M. Esentia, J. Hammond, S. Haszeldine, A. Hosa, S. Shackley, and J. Stewart (2011), Progressing Scotland's CO₂ storage opportunities, *Tech. rep.*, Scottish Carbon Capture and Storage.
- Argent, J., R. Blight, P. Cox, R. Hardy, A. Law, J. R. Smallwood, and D. Walter (2005), The technical challenges to exploration and development of the Kopervik Fairway, Outer Moray Firth, UK, *Geological Society, London, Petroleum Geology Conference series*, 6, 217–229.
- Bastin, J. C., T. Boycott-Brown, A. Sims, and R. Woodhouse (2003), The South Morecambe gas field, blocks 110/2a, 110/3a, 110/7a and 110/8a, East Irish Sea, *Geological Society, London, Memoirs*, 20(1), 107–118.

- Bennion, D. B., and S. Bachu (2008), Drainage and imbibition relative permeability relationships for supercritical CO₂/brine and H₂S/brine systems in intergranular sandstone, carbonate, shale, and anhydrite rocks, *SPE Reservoir Evaluation and Engineering*, 11(3), 487–496.
- Benson, S., R. Pini, C. Reynolds, and S. Krevor (2013), Relative permeability analyses to describe multi-phase flow in CO₂ storage reservoirs, *Tech. rep.*, Global CCS Institute.
- Blunt, M. J. (2017), *Multiphase flow in permeable media A Pore-Scale Perspective*, Cambridge University Press.
- Brownsort, P., V. Scott, G. Sim, and S. Haszeldine (2015), Carbon dioxide transport plans for carbon capture and storage in the North Sea region - a summary of existing studies and proposals applicable to the development of projects of common interest, *Tech. rep.*, Scottish Carbon Capture and Storage.
- Brownsort, P., S. Haszeldine, P. Parmiter, and V. Scott (2016), Scottish CO₂ hub a unique opportunity for the United Kingdom, *Tech. Rep. WP-SCCS 2016-01*, Scottish Carbon Capture and Storage.
- Burnside, N., and M. Naylor (2014), Review and implications of relative permeability of CO₂/brine systems and residual trapping of CO₂, *International Journal of greenhouse gas control*, 23, 1–11.
- Capture Power (2013), White Rose Project.
- Chadwick, A., R. Arts, C. Bernstone, F. May, S. Thibeau, and P. Zweigel (2008), Best practice for the storage of CO₂ in saline aquifers-observations and guidelines from the SACS and CO₂STORE projects, *Tech. rep.*, British Geological Survey.
- Cooke-Yarborough, P. (1991), The Hewett field, blocks 48/28-29-30, 52/4a-5a, UK North Sea, *Geological Society, London, Memoirs*, 14(1), 433–441.
- Cooke-Yarborough, P., and E. Smith (2003), The Hewett fields: Blocks 48/28a, 48/29, 48/30, 52/4a, 52/5a, UK North Sea: Hewett, Deborah, Big Dotty, Little Dotty, Della, Dawn and Delilah fields, *Geological Society, London, Memoirs*, 20(1), 731–739.
- Corbett, P. W. M., P. S. Ringrose, J. L. Jensen, and K. S. Sorbie (1992), Laminated clastic reservoirs: The interplay of capillary pressure and sedimentary architecture, *67th Annual Technical Conference and Exhibition of the Society of Petroleum Engineers, Washington D.C., October 4-7*, (SPE 24699).
- Cowan, G., and T. Boycott-Brown. (2003), The North Morecambe field, block 110/2a, East Irish Sea, *Geological Society, London, Memoirs*, 20(1), 97–105.
- Debbabi, Y., M. Jackson, G. Hampson, and P. Fitch (2016), The interplay of capillary and viscous forces driving flow through layered porous media, *ECMOR XV - 15th European Conference on the Mathematics of Oil Recovery*, (Mo P027).
- Debbabi, Y., M. D. Jackson, G. J. Hampson, and P. Salinas (2017), Capillary heterogeneity trapping and crossflow in layered porous media, *Transport in Porous Media*, pp. 1–24.
- Delprat-Jannaud, F., J. Pearce, M. Akhurst, C. M. Nielsen, F. Neele, A. Lothe, V. Volpi, S. Brunsting, and O. Vinck (2015), SITECHAR methodology for a fit-for-purpose assessment of CO₂ storage sites in europe, *Oil & Gas Science and Technology-Revue d'IFP Energies nouvelles*, 70(4), 531–554.
- Department of Energy and Climate Change (2013), Preferred bidders announced in UK's \$1bn CCS competition, *Press notice 13/028*.
- Department of Energy and Climate Change (2015), HM government statement to markets regarding carbon capture and storage competition, *Press release*.
- Downing, R. A., and D. A. Gray (1986), Geothermal resources of the United Kingdom, *Journal of the Geological Society*, 143(3), 499–507.
- Egermann, P., and R. Lenormand (2005), A New Methodology to Evaluate the Impact of Localized Heterogeneity on Petrophysical Parameters (k_r , P_c) Applied to Carbonate Rocks, *Petrophysics*, 46(5), 335–345.
- Folk, R. L. (1957), *Petrology of sedimentary rocks*, Hemphill Publishing Company.
- Gershenson, N. I., R. W. R. J. D. F. Dominic, E. Mehnert, and R. T. Okwen (2017), Capillary trapping of CO₂ in heterogeneous reservoirs during the injection period, *International*

- Journal of greenhouse gas control*, 59, 13–23.
- Hall, M. R., S. P. Rigby, P. Dim, K. Bateman, S. J. Mackintosh, and C. A. Rochelle (2015), Post-CO₂ injection alteration of the pore network and intrinsic permeability tensor for a permo-triassic sandstone, *Geofluids*, 16(2), 249–263.
- Hangx, S., A. van der Linden, F. Marcelis, and A. Bauer (2013), The effect of CO₂ on the mechanical properties of the Captain Sandstone: geological storage of CO₂ at the Goldeneye field (UK), *International Journal of Greenhouse Gas Control*, 19, 609–619.
- Haszeldine, S., C. Littlecott, and V. Scott (2013), Carbon capture and storage in the UK - response to the energy and climate change select committee call for evidence, *Tech. Rep. WP-SCCS 2013-07*, Scottish Carbon Capture and Storage.
- Hillier, A. P., and B. P. J. Williams (1991), The Leman field, blocks 49/26, 49/27, 49/28, 53/1, 53/2, UK North Sea, *Geological Society, London, Memoirs*, 14(1), 451–458.
- Hingerl, F. F., F. Yang, R. Pini, X. Xiao, M. F. Toney, Y. Liu, and S. M. Benson (2016), Characterization of heterogeneity in the Heletz sandstone from core to pore scale and quantification of its impact on multi-phase flow, *International Journal of greenhouse gas control*, 48, 69–83.
- Holloway, S., and D. Savage (1993), The potential for aquifer disposal of carbon dioxide in the UK, *Energy Conversion and Management*, 34(9), 925–932.
- Holloway, S., C. J. Vincent, M. S. Bentham, and K. L. Kirk (2006), Top-down and bottom-up estimates of CO₂ storage capacity in the United Kingdom sector of the Southern North Sea basin, *Environmental Geosciences*, 13(2), 71–84.
- Huang, Y., P. Ringrose, and K. Sorbie (1995), Capillary trapping mechanisms in water-wet laminated rocks, *SPE Res. Eng.*, 10(4), 287–292.
- Jin, M., E. Mackay, M. Quinn, K. Hitchen, and M. Akhurst (2012), Evaluation of the CO₂ storage capacity of the Captain Sandstone formation, *SPE Europec/EAGE Annual Conference 4-7 June, Copenhagen, Denmark*, (154539-MS).
- Jonoud, S., and M. D. Jackson (2008), New criteria for the validity of steady-state upscaling, *Transport in porous media*, 71, 53–73.
- Ketter, F. (1991a), The Esmond, Forbes and Gordon fields, blocks 43/8a, 43/13a, 43/15a, 43/20a, UK North Sea, *Geological Society, London, Memoirs*, 14(1), 425–432.
- Ketter, F. J. (1991b), The Ravenspurn north field, blocks 42/30, 43/26a, UK North Sea, *The Geological Society, London, Memoirs*, 14, 459–467.
- Kirk, K. L. (2006), Potential for storage of carbon dioxide in the rocks beneath the East Irish Sea, *Tech. Rep. 100*, Tyndall Centre for Climate Change Research.
- Kong, X., M. Delshad, and M. F. Wheeler (2015), History matching heterogeneous coreflood of CO₂/brine by use of compositional reservoir simulator and geostatistical approach, *SPE Journal*, 20(2), 267–276.
- Krause, M., S. Krevor, and S. M. Benson (2013), A procedure for the accurate determination of sub-core scale permeability distributions with error quantification, *Transport in Porous Media*, 98(3), 565–588.
- Krevor, S., M. J. Blunt, S. M. Benson, C. H. Pentland, C. Reynolds, A. Al-Menhali, and B. Niu (2015), Capillary trapping for geologic carbon dioxide storage - from pore scale physics to field scale implications, *International Journal of greenhouse gas control*, 40, 221–237.
- Krevor, S. C. M., R. Pini, B. Li, and S. M. Benson (2011), Capillary heterogeneity trapping of CO₂ in a sandstone rock at reservoir conditions, *Geophysical Research Letters*, 38(L15401).
- Krevor, S. C. M., R. Pini, L. Zuo, and S. M. Benson (2012), Relative permeability and trapping of CO₂ and water in sandstone rocks at reservoir conditions, *Water Resources Research*, 48(2), W02,532.
- Kuo, C.-W., and S. M. Benson (2015), Numerical and analytical study of effects of small scale heterogeneity on CO₂/brine multiphase flow system in horizontal corefloods, *Advances in Water Resources*, 79, 1–17.

- Lach, J. R. (1997), Captain field reservoir development planning and horizontal well performance, *Offshore Technology Conference*, 5-8 May, Houston, Texas, (8508-MS).
- Li, B., and S. M. Benson (2015), Influence of small-scale heterogeneity on upward CO₂ plume migration in storage aquifers, *Advances in Water Resources*, 83, 389–404.
- Manceau, J. C., J. Ma, R. Li, P. Audigane, P. X. Jiang, R. N. Xu, J. Tremosa, and C. Lerouge (2015), Two-phase flow properties of a sandstone rock for the CO₂/water system: Core-flooding experiments, and focus on impacts of mineralogical changes, *Water Resources Research*, 51(4), 2885–2900.
- Mathias, S. A., J. G. Gluyas, G. J. G. M. de Miguel, S. L. Bryant, and D. Wilson (2013), On relative permeability data uncertainty and CO₂ injectivity estimation for brine aquifers, *International Journal of Greenhouse Gas Control*, 12, 200–212.
- McDermott, C., J. Williams, O. Tucker, M. Jin, E. Mackay, K. Edlmann, R. S. Haszeldine, W. Wang, O. Kolditz, and M. Akhurst (2016), Screening the geomechanical stability (thermal and mechanical) of shared multi-user CO₂ storage assets: A simple effective tool applied, *International Journal of Greenhouse Gas Control*, 45, 43–61.
- McPhee, C., J. Reed, and I. Zubizarreta (2015), *Core Analysis: A Best Practice Guide, Developments in Petroleum Science*, vol. 64, Elsevier.
- Meadows, N. S., and A. Beach (1993), Controls on reservoir quality in the triassic Sherwood sandstone of the Irish Sea, *Geological Society, London, Petroleum Geology Conference series*, 4, 823–833.
- Meckel, T., S. Bryant, and P. R. Ganesh (2015), Characterization and prediction of CO₂ saturation resulting from modeling buoyant fluid migration in 2d heterogeneous geologic fabrics, *International Journal of greenhouse gas control*, 34, 85–96.
- Metz, B., O. Davidson, H. de Coninck, M. Loos, and L. Meyer (2005), Carbon dioxide capture and storage, *IPCC special report*, Intergovernmental Panel on Climate Change.
- Niu, B., A. Al-Menhali, and S. C. Krevor (2015), The impact of reservoir conditions on the residual trapping of carbon dioxide in Berea sandstone, *Water Resources Research*, 51, 2009–2029.
- Noy, D. J., S. Holloway, R. A. Chadwick, J. D. O. Williams, S. A. Hannis, and R. W. Lahann (2012), Modelling large-scale carbon dioxide injection into the Bunter sandstone in the UK Southern North Sea, *International Journal of Greenhouse Gas Control*, 9, 220–233.
- Pearce, J. M., S. Holloway, H. Wacker, M. K. Nelis, C. Rochelle, and K. Bateman (1996), Natural occurrences as analogues for the geological disposal of carbon dioxide, *Energy Conversion and Management*, 37(6), 1123–1128.
- Pettijohn, F., P. Potter, and R. Siever (2012), *Sand and Sandstone*, Spring Science & Business Media.
- Pickup, G., and K. Stephen (2000), An assessment of steady-state scale-up for small-scale geological models, *Petroleum Geoscience*, 6, 203–210.
- Pini, R., and S. M. Benson (2013a), Simultaneous determination of capillary pressure and relative permeability curves from core-flooding experiments with various fluid pairs, *Water Resources Research*, 49(6), 3516–3530.
- Pini, R., and S. M. Benson (2013b), Characterization and scaling of mesoscale heterogeneities in sandstones, *Geophysical Research Letters*, 40(15), 3903–3908.
- Pini, R., S. C. Krevor, and S. M. Benson (2012), Capillary pressure and heterogeneity for the CO₂/water system in sandstone rocks at reservoir conditions, *Advances in Water Resources*, 38, 48 – 59.
- Rabinovich, A., K. Itthisawatpan, and L. J. Durlofsky (2015), Upscaling of CO₂ injection into brine with capillary heterogeneity effects, *Journal of Petroleum Science and Engineering*, 134(C), 60–75.
- Ramakrishnan, T. S., and A. Capiello (1991), A new technique to measure static and dynamic properties of a partially saturated porous medium, *Chemical Engineering Science*, 46(4), 1157–1163.
- Reynolds, C. A., and S. Krevor (2015), Characterizing flow behavior for gas injection: Relative permeability of CO₂-brine and N₂-water in heterogeneous rocks, *Water Resources*

- Research*, 51(12), 9464–9489.
- Riches, H. (2003), The Viking field, blocks 49/12a, 49/16, 49/17, UK North Sea, *Geological Society, London, Memoirs*, 20(1), 871–880.
- Ringrose, P., and M. Bentley (2015), *Reservoir Model Design A Practitioners Guide*, Springer.
- Ringrose, P., K. Sorbie, P. Corbett, and J. Jensen (1993), Immiscible flow behaviour in laminated and cross-bedded sandstones, *Journal of Petroleum Science and Engineering*, 9, 103–124.
- Rose, P. (1999), Reservoir characterization in the Captain field: integration of horizontal and vertical well data, *Geological Society, London, Petroleum Geology Conference series*, 5, 1101–1113.
- Ruprecht, C., R. Pini, S. Falta, R. Benson, and L. Murdoch (2014), Hysteretic trapping and relative permeability of CO₂ in sandstone at reservoir conditions, *International Journal of Greenhouse Gas Control*, 27, 15–27.
- Saadatpoor, E., S. L. Bryant, and K. Sepehrnoori (2009), New trapping mechanism in carbon sequestration, *Transport in Porous Media*, 82(1), 3–17.
- Scottish Carbon Capture and Storage (2009), Opportunities for CO₂ storage around Scotland - an integrated strategic research study, *Tech. rep.*, Scottish Carbon Capture and Storage.
- Scottish Carbon Capture and Storage (2011b), Geomechanics summary report, *Tech. Rep. ukccs-kt-s7.19-shell-004*, UK Carbon Capture and Storage Demonstration Competition.
- Scottish Carbon Capture and Storage (2012), Central North Sea - CO₂ storage hub: Enabling CCS deployment in the UK and Europe, *Tech. rep.*, Scottish Carbon Capture and Storage.
- ScottishPower CCS Consortium (2011a), Static model field report, *Tech. Rep. ukccs-kt-s7.21-shell-002*, UK Carbon Capture and Storage Demonstration Competition.
- Shell UK Limited (2013), Peterhead CCS project.
- Shell UK Limited (2015), Peterhead CCS project announcement.
- Smith, M., D. Campbell, E. Mackay, and D. Polson (2012), CO₂ aquifer storage site evaluation and monitoring: Understanding the challenges of CO₂ storage: results of the CASSEM project, *Tech. rep.*, Scottish Carbon Capture and Storage.
- Stuart, I. A. (1993), The geology of the North Morecambe gas field, East Irish Sea basin, *Geological Society, London, Petroleum Geology Conference series*, 4, 883–895.
- Stuart, I. A., and G. Cowan (1991), The South Morecambe Field, blocks 110/2a, 110/3a, 110/8a, UK East Irish Sea, *Geological Society, London, Memoirs*, 14(1), 527–541.
- Szulczewski, M. L., C. W. MacMinn, H. J. Herzog, and R. Juanes (2012), Lifetime of carbon capture and storage as a climate-change mitigation technology, *Proceedings of the National Academy of Sciences of the United States of America*, 109(14), 5185–5189.
- Underhill, J. R., N. Lykakis, and S. Shafique (2009), Turning exploration risk into a carbon storage opportunity in the UK Southern North Sea, *Petroleum Geoscience*, 15(4), 291–304.
- Virnovsky, G. A., H. A. Friis, and A. Lohne (2004), A steady-state upscaling approach for immiscible two-phase flow, *Transport in Porous Media*, 54, 167–192.
- Wentworth, C. (1922), A scale of grade and class terms for clastic sediments, *The Journal of Geology*, 30(5), 377–392.
- White Rose Project (2015), Yorkshire and Humber CCS project: The opportunity, *Tech. rep.*, National Grid.
- Williams, J. D. O., S. Holloway, and G. A. Williams (2014), Pressure constraints on the CO₂ storage capacity of the saline water-bearing parts of the Bunter Sandstone formation in the UK Southern North Sea, *Petroleum Geoscience*, 20(2), 155–167.
- Yokoyama, Y., and L. Lake (1981), The effects of capillary pressure on immiscible displacements in stratified porous media, *56th Annual Fall Technical Conference and Exhibition of the Society of Petroleum Engineers of AIME, San Antonio, Texas, October 5-7*, (SPE 10109).

- Yoshida, N., J. S. Levine, and P. H. Stauffer (2016), Investigation of uncertainty in CO₂ reservoir models: A sensitivity analysis of relative permeability parameter values, *International Journal of Greenhouse Gas Control*, 49, 161–178.
- Zhou, D., F. Fayers, and F.M. Orr, Jr. (1997), Scaling of multiphase flow in simple heterogeneous porous media, *SPE Reservoir Engineering*, 12(3), 559–569.